Cellulose
https://doi.org/10.1007/s10570-019-02849-4

ORIGINAL RESEARCH

Influence of post-oxidation reactions on the physicochemical properties of TEMPO-oxidized cellulose nanofibers before and after amidation

L. A. Calderón-Vergara · S. A. Ovalle-Serrano · C. Blanco-Tirado · M. Y. Combariza

Received: 23 April 2019 / Accepted: 8 November 2019

Abstract During TEMPO-mediated oxidation of cellulose, primary alcohols on the surface ideally undergo oxidation to carboxylic acids. However, it is well known that some of these hydroxyl groups partially oxidize to aldehydes. To increase the degree of oxidation (DO) of nanocellulose, these unreacted aldehydes can be fully oxidized to carboxylic acids employing various strategies. We performed post-oxidation reactions using $NaClO_2$, on TEMPO-Oxidized Cellulose Nanofibers (TOCN) to investigate how this reaction influenced the physicochemical properties of nanocelulose before and after amidation with octadecylamine (ODA). We report on an increase in the content of carboxylate in TOCN (1.57 mmol/g of cellulose) up 40% after post-oxidation with $NaClO_2$ (2.20 mmol/g of cellulose). These results indicate that with TEMPO-mediated oxidation, 1.57 mmol of hydroxymethyl groups per gram of cellulose were completely oxidized to –COOH, and after treatment with $NaClO_2$, about 0.63 mmol of partially-oxidized alcohols (aldehyde groups) on TOCN were fully oxidized to COOH. Theoretical HLB values of 11.04 and 11.13 for TOCN and post-oxidized TOCN (TOCN-P) indicate that these materials behave as hydrophilic o/w surfactants or emulsifying agents with high affinity for polar phases. They also form highly stable dispersions in water due to an increased charge density as indicated by ζ-potential values of -56 mV for TOCN and -64 mV for TOCN-P. Low contact angles (CA) of 24º and 21º for TOCN and TOCN-P films confirm their hydrophilic nature. After amidation reactions with ODA, we observe a 73% and an 82% decrease in carboxylate content for TOCN and TOCN-P. These values can be related with the degree of coupling (DC) leading to amide formation on the nanocellulose surface, *i.e.,* about 1.14 and 1.80 mmol of amide units were coupled per gram of cellulose on TOCN-ODA and TOCN-P-ODA. ζ-potential values decreased 34% and 52% after amidation, to -37 mV and -31 mV for TOCN-ODA and TOCN-P-ODA, indicating a low stability of these materials in water dispersions. Theoretical HLB values < 8.6 suggest the ability of these materials to act as wetting/spreading agents with poor dispersibility in water. In addition, high CA (> 125º) films illustrate the effect of octadecylamine alkyl chains on the hydrophobic properties of the nanocellulose's surface. Thermal analysis indicates that amidation reactions can effectively shield in the nanocellulose's surface from thermal degradation from by increasing the decomposition temperature from around 296 °C for "naked"

Electronic supplementary material The online version of this article (https://doi.org/10.1007/s10570-019-02849-4) contains supplementary material, which is available to authorized users.

L. A. Calderón-Vergara · S. A. Ovalle-Serrano · C. Blanco-Tirado · M. Y. Combariza (✉)
Escuela de Química, Universidad Industrial de Santander, Bucaramanga 680002, Colombia
e-mail: marianny@uis.edu.co

Published online: 19 November 2019

TOCN to > 330 °C for the "protected" amidated nanocellulose.

Keywords TEMPO-oxidized cellulose nanofibers, TOCN, post-oxidation · $NaClO_2$ · Octadecylamine · Amidation · Surface free energy (SFE)

Introduction

TEMPO-mediated oxidation, widely used to produce oxidized cellulose nanofibers (TOCN), involves the selective oxidation of C6–OH groups to carboxylates, through an intermediate aldehyde. TEMPO involves the addition of a primary oxidant (*e.g.* NaClO) to aqueous suspensions of delignified cellulose containing the 2,2,6,6-tetramethylpiperidine-1-oxyl radical (TEMPO) and a co-oxidant (*e.g.* NaBr) under basic conditions (Saito et al. 2006). TEMPO oxidation occurs superficially in the crystalline and amorphous regions of cellulose. After oxidation, the carboxylic units in TOCN are in the form of sodium salts (-COONa) thus facilitating defibrillation by electrostatic repulsions (Benkaddour et al. 2014). However, a certain amount of primary alcohols is incompletely oxidized in TOCN leaving aldehyde units, about 0.6 mmol/g of cellulose (Isogai et al. 2010). These aldehyde units may interfere in the defibrillation and in subsequent surface chemical modifications of nanocellulose (Saito and Isogai 2004; Gert et al. 2005). Several strategies have been reported for the preparation of nanocellulose with a high carboxylate content including the treatment of pulp with NaOH/urea prior to TEMPO oxidation (Tang et al. 2017). More recently, a simpler alternative to produce aldehyde-free pulps with a high content of carboxyl groups includes the post-oxidation with sodium chlorite ($NaClO_2$) in acid medium (Isogai et al. 2018).

The carboxylate content of TOCN and post-oxidized TOCN (TOCN-P) is related to the degree of oxidation (DO) of cellulose surface after TEMPO and the selective post-oxidation with $NaClO_2$. TOCN and TOCN-P from sources such as microfibrillated cellulose and residual biomass exhibit a carboxylate content ranging from 0.8 to 1.8 mmol COOH/g cellulose (Saito et al. 2006; Isogai et al. 2010). Increasing DO in TOCN, by means of soft post-oxidation strategies to selectively convert aldehydes into carboxylate groups, is fundamental to obtain more hydrophilic materials (Rodionova et al. 2012; He et al. 2014; Xiao et al. 2015). While post-oxidation reactions have been used to determine the aldehyde content in oxidized cellulose fibers (Saito and Isogai 2004; Saito et al. 2005), the physicochemical changes that TOCN may suffer after post-oxidation have not been studied in detail. More importantly, the possibility of using post-oxidation as a way to increase the hydrophobicity of nanocellulose have not been fully explored yet.

Hydrophobization is key to overcome issues, such as low adhesion and weak interfacial interaction, that prevent hydrophilic TOCN from being used as reinforcement of non-polar polymer matrices in composites (Bhatnagar 2005). So far, hydrophobic TOCN has been obtained by using a wide variety of methods involving the formation of ionic and covalent bonds via chemical esterification, silylation and amidation (Bledzki et al. 2008; Xu et al. 2009; Benkaddour et al. 2014). Cellulose amidation reactions usually require the use of coupling agents such as water-soluble carbodiimides like EDC [1-ethyl-3-(3-dimethylaminopropyl) carbodiimide] or its analogs (EDAC, DCC) and NHS (N-hydroxysuccinimide) which promote the formation of a stable carboxylamine conjugated system (Sehgal 1994). However, these processes are slow, require high temperatures, specific pH values and multiple stages. Our group reported a fast and efficient 'one-pot' amidation reaction to produce hydrophobic TOCN from commercial microcrystalline cellulose (Gómez et al. 2017). This approach allowed for the modification of up to 70% of the superficial carboxylic units (1.25 mmol COOH/g of cellulose) with long alkyl chain primary amines (dodecylamine and octadecylamine) using TBTU (an uronium salt) as amidating agent. However, this process yields a material with high wettability CA of 67°. The low hydrophobicity of the material could be due to a low degree of oxidation (DO) of the starting TOCN or to a low degree of coupling (DC) during the amidation reaction.

We seek to obtain functional hydrophobic materials using agro-waste from the Colombian Fique industry, so we used Fique tow as cellulose source to produce TOCN via TEMPO oxidation. TOCN was in turn post-oxidized with $NaClO_2$ to increase its DO

(TOCN-P). The two materials were rendered hydrophobic by a 'one-pot' amidation reaction with ODA. From initial contact angles of 21 and 24 degrees for the hydrophilic TOCN and TOCN-P, we registered 126 and 130 degrees for the hydrophobic amidated materials. This observation indicates that post oxidation of TOCN with $NaClO_2$, which increases the amount of carboxylate units on the surface of nanocellulose from 1.57 mmol/g of cellulose in TOCN to 2.20 mmol/g of cellulose in TOCN-P, is an effective strategy to increase nanocellulose hydrophobicity.

Experimental

Materials

Fique tow (*Furcraea macrophylla*) was collected from decorticated Fique leaves in the rural area of San Joaquín, Santander, Colombia. 2,2,6,6-Tetramethylpyperidin-1-oxyl (TEMPO) was purchased from Sigma Aldrich (Saint Louis, MO, USA) and sodium hypochlorite (NaClO, 15%) from Carlo Erba Reagents (Milan, Italy). Sodium bromide (NaBr), hydrogen peroxide (H_2O_2), sodium hydroxide (NaOH), sodium chlorite ($NaClO_2$, 25%), ethanol (EtOH), methanol (MeOH), N'N-dimethyl-formamide (DMF), 3,7-bis (Dimethylamino)-phenothiazin-5-ium chloride (methylene blue (MB)), acetic acid (glacial) and hydrochloric acid (HCl, 37%) were purchased from Merck (Darmstadt, Germany). [O-(1Hbenzotriazol-1-yl)-N,N,N',N'-tetramethyluronium tetrafluoroborate] (TBTU) 97% was purchased from Chempep (Wellington, FL, USA). All chemical reagents were used with no further purification. Aqueous solutions and suspensions were prepared with ultrapure water (18 MΩ•cm @ 25 °C).

Fique tow treatment

Fique tow specimens were immersed for 60 min at 40 °C in an ultrasound bath (Bransonic CPX3800, 40 kHz, 130 Watt) of distilled water to remove residues and minerals such as carbonates and oxalates. The sonicated fique tow was dried in an oven at 60 °C for 24 h (Ovalle-Serrano et al. 2018a) and labelled as "untreated Fique tow". To remove non-cellulosic compounds such as hemicellulose and lignin, we used a procedure reported before (Ovalle-Serrano et al. 2018a). In brief, untreated Fique tow was cut into short lengths (1 cm) and 8 g were immersed in 100 mL of a H_2O_2 solution (10% w/w), which was rendered basic (pH 11.5) by dropwise addition of NaOH (4 N). The mixture was kept in an ultrasonic bath for 2 h at 70 °C. After completion of the AHP (Alkaline hydrogen peroxide) treatment, the delignified material was washed with distilled water and dried at 60 °C for 24 h. Untreated Fique tow (Figure S1**)** is a light-yellow material with a rigid texture due to its high lignin content (23.9%). After the removal of hemicellulose and lignin the color of Fique tow turns into white (Fig. 1) as it has a cellulose content up to 90% (Ovalle-Serrano et al. 2018a).

TEMPO-mediated oxidation and mechanical disintegration

We followed a procedure reported by Saito and Isogai (Saito and Isogai 2004) using the TEMPO/NaClO/NaBr system, with slightly modifications (Ovalle-Serrano et al. 2018b). 1 g of delignified Fique tow was immersed into 100 mL of water. TEMPO (16 mg) and sodium bromide (100 mg) were dissolved in distilled water and added slowly to the beaker containing the tow. NaClO (0.037 mol) was added dropwise to start the oxidation reaction which was carried out on an ultrasonic bath (Bransonic CPX3800, 40 kHz, 130 Watt), keeping the pH at 10.5 at room temperature. When the oxidation process ended (no need for addition of NaOH to maintain the pH) the reaction was stopped by the adding ethanol. The oxidized cellulose was centrifuged at 4700 rpm for 15 min with ultrapure water until neutral pH to separate the TOCN. Fique tow TOCN aqueous suspensions of 0.5% wt were mechanically disintegrated by sonication in an Ultrasonic Processor (Sonics vibra-cell VC750, 20 kHz, 750 Watt) for 10 min (1:1 pulses) at 40% power. After sonication, the product was centrifuged and the soluble fraction in water (supernatant) was stored for characterization.

TOCN post-oxidation with $NaClO_2$

During the TEMPO-mediated oxidation of cellulose, under basic conditions, primary alcohols ideally undergo oxidation to carboxylic acids. However, some of these hydroxyl groups only partially oxidize to

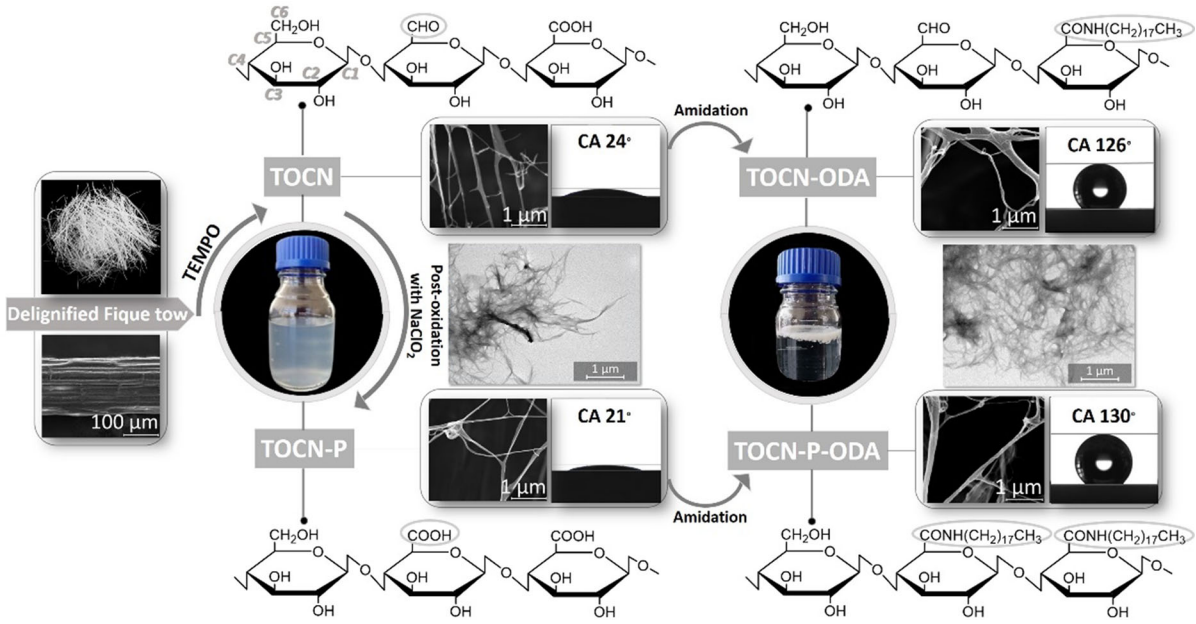

Fig. 1 General scheme for TOCN isolation, post-oxidation and hydrophobization

aldehydes. The unreacted aldehydes were fully oxidized to carboxylic acids using a slightly modified procedure initially reported by Mishra et al. (Mishra et al. 2012). In short, 2 g of Fique tow TOCN were oxidized with $NaClO_2$ (20 mL, 25% w/w) and acetic acid at pH 3–4. The mixture was diluted to a final concentration of 1% w/v by adding water and allowing it to react for 2 h at 40 °C. Finally, the post-oxidized Fique TOCN (TOCN-P) specimens were cooled at room temperature and washed thoroughly with ultrapure water. After post-oxidation, the increase in the carboxyl content was directly correlated with the aldehyde content in the original Fique TOCN.

TOCN and TOCN-P amidation reactions

Suspensions of oxidized nanocellulose (TOCN-COONa and TOCN-P-COONa) were coupled to octadecylamine (ODA) using a procedure previously reported by Gómez et al. (Gómez et al. 2017). TOCN and TOCN-P suspensions (100 mL 1% wt.) were mixed with TBTU salt (2:1 molar radio TBTU: TOCN) previously dissolved in DMF under stirring for 30 min at room temperature. An octadecylamine solution (4:1 molar ratio amine–COOH group) was added and the mixture was allowed to react for 2 h under constant stirring at room temperature. When the reaction was finished, the product, a light-yellow supernatant, migrated to the surface. The final products, labeled as TOCN-ODA and TOCN-P-ODA, were vacuum filtrated with methanol, HCl (0.01 M) and water.

Conductimetry

The degree of oxidation (DO), the surface charge density or carboxylate content (σ mmol COOH/g cellulose) and the degree of coupling after the amidation process (DC) of the cellulose (untreated Fique tow, delignified Fique tow, TOCN, TOCN-P, TOCN-ODA and TOCN-P-ODA) were measured by a conductimetric titration method according to a procedure reported by Habibi et al. (Habibi et al. 2006). 50 mg of the sample were suspended in a 0.01 M HCl solution until pH 2 and stirred for 15 min. The suspensions were then titrated with a 0.01 M NaOH solution. All experiments were carried out in triplicate. Generally, conductimetric titration curves show two inflection or equivalent points: the first one indicates the neutralization of the strong acid, HCl, in this region the conductance of the

solution decreases rapidly due to the displacement of H^+ by Na^+ cations; the second point represents the neutralization of the weak acids, -COOH, in this region the conductance remains constant. When both acids have been completely neutralized, the conductivity increases due to the excess of OH^- ions from the base (Smith et al. 2010). The volume of NaOH used to neutralize the carboxylic groups in the cellulose samples allows calculation of DO, σ and DC as shown in the following equations:

$$DO = 162(V_2 - V_1)c[m - 36(V_2 - V_1)c]^{-1} \quad (1)$$

$$\sigma = [c(V_2 - V_1)]m^{-1} \quad (2)$$

$$DC = DO_{(TOCN(P)-ODA)} - DO_{(TOCN(P))} \quad (3)$$

where c is the concentration (mol/L) of the titrant solution, V_1 and V_2 is the volume (L) of NaOH needed to neutralize the strong and weak acids, respectively, and m is the mass of the sample (g). In Eq. 3, the subscripts TOCN (P) and TOCN (P) - ODA refer to TOCN and TOCN-P before and after the amidation reaction, respectively.

Dispersibility tests

0.01 g of nanocellulose (TOCN, TOCN-P, TOCN-ODA and TOCN-P-ODA) were added to a glass vial and solvents were added to obtain concentrations of 0.2% w/v. The mixtures were stirred at room temperature for 2 h (1500 rpm). UV transmittance measurements from 285 to 750 nm, using a Shimadzu UV–Vis spectrophotometer (UV-2401PC), were used to determine the solubility of the mixtures (Saito et al. 2007).

Characterization

IR-ATR spectra were collected using a Bruker Tensor 27 Fourier transform infrared (IR-ATR) spectrometer equipped with a Platinum Diamond ATR unit A225/Q (Billerica, MA). A total of 32 scans were acquired for each spectrum at a resolution of 2 cm^{-1} (4000-500 cm^{-1}). Figure S2 shows the success of delignification of the untreated Fique tow before being subjected to TEMPO oxidation. Crystalline properties were analyzed by X-ray diffraction (XRD) spectroscopy on a Bruker D8 DISCOVER X-ray diffractometer (Billerica, MA) with a DaVinci geometry (CuKα1 radiation (k= 1.54 Å), 40 kv/40 mA) using an area detector VANTEC-500 and a poly (methyl methacrylate) sample holder. Contact angle measurements, using the sessile drop technique (1 µL of deionized water) on film samples, were carried out on an OCA 15EC contact angle system (Data Physics, Filderstadt, Germany) equipped with a dosing syringe (Lif et al. 2010). TOCN, TOCN-P, TOCN-ODA and TOCN-P-ODA films were casted by placing 200 µL of 1% w/w suspensions of each sample (TOCN derivatives in water and TOCN-amidated derivatives in toluene) onto microscopy glass slides treated with a 3:1 sulfuric acid:hydrogen peroxide mixture. The films were dried at room temperature for 24 h. All measurements were performed by triplicate with an accuracy of 0°–180°±0.1 for contact angle measurement. In addition, the dispersive and polar components of the surface free energy for each material were calculated using the Owens, Wendt, Rabel and Kaelble method (Zenkiewicz 2006; Khoshkava and Kamal 2013; Bashar et al. 2017; Sun et al. 2018; Hasan et al. 2019). Thermal decomposition curves (TGA) of freeze-dried samples (10 mg) were probed using a STA 449 F5 Jupiter instrument (São Paulo, Brazil) under nitrogen (50 mL/min). The samples were scanned from room temperature up to 500 °C at a heating rate of 10 °C/min. Surface morphology was studied by field emission scanning electron microscopy (FESEM) using a FEI QUANTA FEG 650 (Oregon, USA) instrument operated at 20 kV and equipped with a large field detector. Samples were coated with gold using a Quorum 150T ES system (Oregon, USA). Zeta-potential (ζ) measurements were made using a Malvern Zetasizer Nano ZS90 instrument (Worcestershire, UK) equipped with a capillary cell 1070. TEM images were collected on a FEI Tecnai T12 Spirit TEM (FEI, Hillsboro, OR) with an acceleration voltage of 120 keV. Samples for TEM imaging were drop casted onto carbon coated copper grids and left to dry at ambient conditions.

Results and discussion

TOCN isolation, post-oxidation, and hydrophobization

Figure 1 illustrates the process for TOCN isolation (from Fique tow), post-oxidation ($NaClO_2$), hydrophobization by amidation (octadecyl amine, ODA), and the appearance of the resultant materials (at macro and micro scales) as well as a schematic

representation of the chemical structure. We have previously characterized fique tow and have also demonstrated that delignification is fundamental to increase Fique TOCN yields after TEMPO (Ovalle-Serrano et al. 2018b). Fique TOCN synthesis via TEMPO involves a catalytic series of oxidation–reduction reactions, starting with NaBr oxidation by NaClO to sodium hypobromite (NaOBr) followed by transformation of TEMPO (or a related stable radical) into a nitrosonium ion capable of selectively oxidizing primary hydroxyls from cellulose to aldehyde while reducing to hydroxylamine (Akira Isogai 2011). The aldehyde group produced in the first step of the reaction is oxidized to carboxylic acid by the same process, because the nitrosonium ion can be regenerated from the hydroxylamine hence completing the catalytic cycle (Bragd et al. 2000), see Scheme S1 of the Supporting Information. Two molar equivalents of NaClO are needed to oxidize one molar equivalent of primary –OH to –COOH (Yang 2011). In addition, the use of ultrasound energy has a significant impact on the TEMPO-mediated oxidation reaction, since it can gradually disintegrate the micron-sized cellulose fibers into nanofibers depending on the treatment conditions (Chen et al. 2011; Dai et al. 2015; Ovalle-Serrano et al. 2018b). After the TEMPO-mediated oxidation of delignified Fique tow followed by mild post-oxidation with $NaClO_2$, to transform partially oxidized aldehydes into carboxylic acids, we observed stable aqueous suspensions of TOCN and TOCN-P. Oxidation of primary hydroxyls to carboxylic acids in the anhydroglucose units of cellulose occurs through an intermediate aldehyde (as seen in Scheme S1). Some reports state that not all aldehydes are oxidized to acids during the TEMPO-mediated oxidation and that small amounts of these groups remain on the final TOCN (Kato et al. 2003; Sun et al. 2005; Mishra et al. 2012). Interestingly, aldehydes in TOCN are not only the result of incomplete oxidation of primary hydroxyls but can also be consequence of secondary reactions involving C2-C3 cleavage of anhydroglucose units (forming aldehydes and dicarboxylic structures) promoted by NaClO during TEMPO oxidation (Besemer 1993; Bragd et al. 2000). In addition, formation of intra and intermolecular hemiacetals with hydroxyls groups from other cellulose chains also prevents the complete oxidation of the aldehydes by steric hindrance (Saito and Isogai 2004).

To increase the amount of carboxyl groups in Fique TOCN, we transformed the remaining aldehydes into carboxyl groups by a mild post-oxidation reaction with $NaClO_2$ and acetic acid at pH 3–4 (Scheme 1). $NaClO_2$ has been widely used to specifically oxidize aldoses to aldonic acids. In this reaction, an acidic medium guarantees inhibition of secondary oxidation reactions of alditols and ketoses (Mishra et al. 2012). $NaClO_2$ is in equilibrium with conjugated chlorous acid ($HClO_2$), which is the entity responsible for the oxidation of the aldehydes to carboxylic acids (as seen in Scheme 1) (David R. Williams 1980).

Figure 1 also shows the hydrophobic characteristics of TOCN-ODA and TOCN-P-ODA The amidation of TOCN and TOCN-P occurs under alkaline conditions, by a reaction between superficial carboxylate anions in TOCN and TOCN-P with an electronically deficient uronium salt -TBTU [O- (1H-benzotriazol-1-yl)-N,N,N',N'-tetramethyluronium tetrafluoroborate]- forming an N-oxime active ester. The active ester reacts (by nucleophilic addition) with a primary amine (octadecylamine) forming an amide bond (Gómez et al. 2017). The hydrophobicity is achieved in this case by lowering the surface energy of the nanocellulose by using long alkyl-chains covalently attached to the surface.

Nanocellulose characterization

FESEM images in Fig. 1 show characteristic networks for Fique TOCN, TOCN-P, TOCN-ODA and TOCN-P-ODA. These images show that the surface modification with alkyl chains of TOCN-P and TOCN does not significantly change the morphology of the material. Similar observations were reported by Missoum et al. after modification with long aliphatic isocyanate chains (Missoum et al. 2012). Also, TEM images of TOCN and TOCN-ODA in Fig. 1 show nanofiber widths ranging from 10 to 20 nm and lengths of several micrometers. TEM of TOCN-P and TOCN-P-ODA display similar sizes and morphology.

In Fig. 2 the IR spectra show changes in the surface chemistry of the nanocellulose specimens (TOCN, TOCN-P, TOCN-ODA and TOCN-P-ODA). Characteristic cellulose signals are common to all spectra; for instance, a wide band in the region of

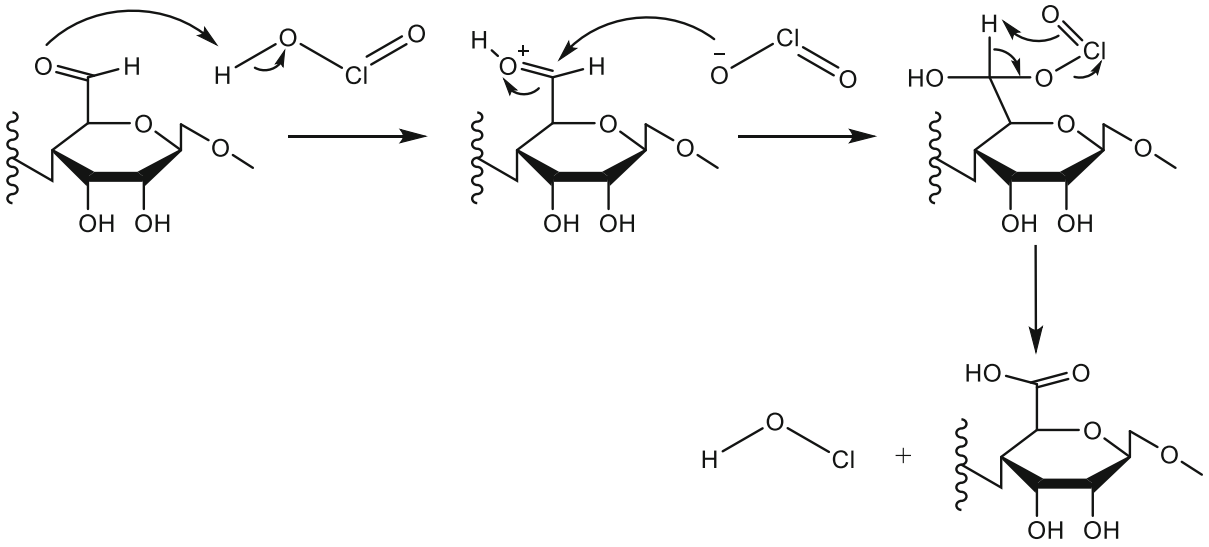

Scheme 1 The Post-oxidation mechanism for TOCN, using $NaClO_2$ as mild oxidant

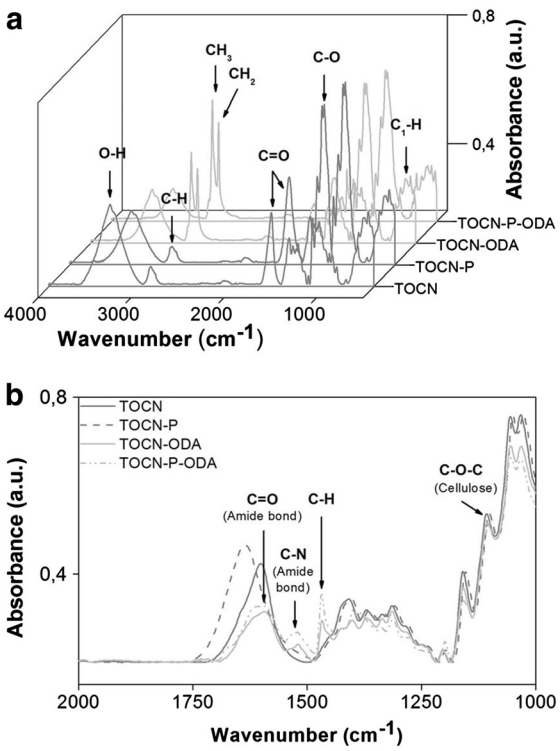

Fig. 2 IR-ATR spectra of nanocellulose specimens obtained from fique fibers (TOCN–COONa, TOCN-P, TOCN-ODA and TOCN-P-ODA)

3000–3500 cm^{-1} is attributed to O–H stretching vibrations (Iskalieva et al. 2012). Signals at 2896, 1600 and 1426-1318 cm^{-1} correspond to symmetric and asymmetric vibrations of the C-H unit, H–O-H stretching vibrations of absorbed water and the C6-H_2 flexion of the hydroxymethyl unit in the glucopyranose ring. The most prominent band in the IR spectra corresponds to the glucosidic bond β (1→4) C–O–C stretching vibration between 1203 and 1108 cm^{-1} and to the C-O vibration of C2, C3 and C6 at 1028 cm^{-1}. Finally, a small signal at 897 cm^{-1} is originated from C1–H anomeric carbon (Chen et al. 2011).

The IR spectra for TOCN and TOCN-P exhibit signals characteristic of cellulose surface oxidation. The signal at 1602 cm^{-1} represents the C=O stretching vibration characteristic of carbonyl groups of aldehydes (COH) and carboxylates (COO^-) in TOCN-COONa (Tang et al. 2017). After TOCN post-oxidation with $NaClO_2$, we observe a shift in the C=O vibration band to a lower energy (1637 cm^{-1}). This could be due to the presence of only carbonyl groups in TOCN-P. After amidation of TOCN and TOCN-P two characteristic signals of the amide group emerge: amide I and amide II at 1592 and 1520 cm^{-1}, respectively. For TOCN-ODA the amide I signal is due to the C=O stretching in amides, that to some extent overlaps with the stretching vibration of C=O of the remaining aldehydes and carboxylates, and the amide II representing the stretching and deformation of the NH moiety (Lasseuguette 2008). For TOCN-P-ODA, the amide I band overlaps with another signal at 1617 cm^{-1} assigned to the C=O

stretching vibration of unreacted carboxylate groups. In addition, the formation of amide bonds in TOCN-ODA and TOCN-P-ODA was verified by intense signals at 2849 and 2916 cm^{-1}, attributed to the stretching vibrations of the $–CH_3$ and $–CH_2$ groups of the octadecyl alkyl chains (Fig. 2a). A new signal also appeared at 1468 cm^{-1} due to CH deformation of the C_{18} chain from ODA (Benkaddour et al. 2014).

TOCN isolation, post-oxidation and hydrophobization reactions may impact the structure of cellulose. The crystallinity index (CrI) can be used as a parameter to determine how the cellulose crystallinity was affected by the different processes of isolation and modification. CrI, calculated according to the Segal method, relates to the relative amount of crystalline and amorphous material in cellulose (Segal et al. 1959). Figure 3 shows the X-ray diffraction profiles of the nanocellulose specimens isolated from Fique tow. The diffraction patterns in Fig. 3 coincide with the representative crystallographic planes of cellulose type I as reported by the Joint Committee on Powder Diffraction Standards (JCPDS fi le, No. 50-2241), space group P21 (No 4) (Morán et al. 2008; Mandal and Chakrabarty 2011; Sèbe et al. 2012). The first broad band at 15.32° corresponds to the overlapping of the signals of crystallographic planes (010) Iα, (1-10) I β and (100) Iα, (110) Iβ. The most intense signal at 22.5° represents the crystallographic planes (110) Iα and (200) Iβ (Okita et al. 2010; French 2014) and finally the weakest peak at 34.4° is due to multiple reflections including the (11-4) Iα and (004) Iβ which corresponds to one-fourth of the crystallographic

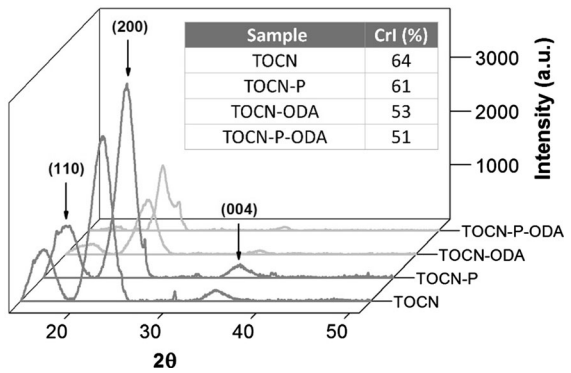

Fig. 3 X-ray diffraction profiles for the TOCN, TOCN-P, TOCN-ODA and TOCN-P-ODA specimens

fiber repeat or c-axis spacing (Wada et al. 2003; Davidson et al. 2004; French 2014).

The raw material, Fique tow, exhibits a significant increase in crystallinity after delignification (CrI changes from 60 to 67% as shown in Figure S3). The increase in crystallinity was due to the removal of amorphous materials such as hemicellulose and lignin after AHP treatment (Ovalle-Serrano et al. 2018a). After TEMPO-mediated oxidation, carboxyl groups are introduced mainly into the amorphous regions of cellulose as they are more reactive than those in the crystalline regions (Benkaddour et al. 2014). The diffraction profile of TOCN derivatives in Fig. 3 shows no changes, when compared with the pattern of the raw material. This indicates that the surface modification treatments (oxidation and post-oxidation) had no effect in the polymeric macrostructure (Johnson et al. 2011). However, a slight decrease in crystallinity (CrI) was observed for TOCN and TOCN-P at 64% and 61%, as a consequence of the introduction of carboxylate groups and the use of ultrasound energy employed to the separation of the nanofibers (Gómez et al. 2017). This small decrease in crystallinity indicates that post-oxidation was mild enough to oxidize the aldehydes present in the TOCN without dramatically affecting the structure of the nanofibers. Interestingly, an increase in the crystallinity of cellulosic pulps has been reported after post-oxidation (Mishra et al. 2012), possibly due to hydrolysis of the amorphous regions on the nanofibers. The post-oxidation conditions used in this report may be responsible for this decrease in CrI (Mishra et al. 2012), since the reaction temperature was reduced (from 70, as reported in literature, to 40 °C) to avoid the loss of amorphous regions. On the other hand, after TOCN/TOCN-P modification the crystallinity index dropped to 53% and 51% for TOCN-ODA and TOCN-P-ODA. This drop is probably due to the introduction of long octadecyl alkyl chains (Gómez et al. 2017).

Cellulose oxidation is accompanied by increased dispersibility of the material in polar solvents. Thus, conductometric measurements of dispersible cellulosic materials are used to measure the extent of surface modification in terms of degree of oxidation (DO), surface charge density or carboxylate content (σ mmol COOH/g cellulose) and degree of coupling after the amidation process (DC) as shown in Table 1. The untreated and the delignified Fique tow

Table 1 Degree of oxidation (DO), degree of coupling after amidation process (DC), carboxylate content (σ) and ζ-potential of Fique tow nanocellulose specimens: TOCN, TOCN-P, TOCN-ODA and TOCN-P-ODA

Material	DO	DC	σ(mmol COOH/g cellulose)	C6-oxidized AGU/1000 AGU	ζ-potential (-mV)
TOCN	0.29	–	1.57	254	56
TOCN-P	0.39	–	2.20	356	64
TOCN-ODA	0.07	0.22	0.43	69	37
TOCN-P-ODA	0.06	0.33	0.40	64	31

specimens, exhibit low DO values (0.04 and 0.07, respectively), indicating the presence of small amounts of carboxylic groups in the samples (see Table S1 of the Supporting Information).

After oxidation and post-oxidation, TOCN and TOCN-P DO values were determined at 0.29 and 0.39 which are equivalent to a σ of 1.57 and 2.20 mmol/g of cellulose. This means that after the TEMPO-mediated oxidation, 1.57 mmol of hydroxymethyl groups per gram of cellulose were oxidized to carboxylate groups and about 0.63 mmol of remaining aldehyde groups after TEMPO, were oxidized to their respective carboxylic acids after treatment with $NaClO_2$. To our knowledge, the DO and σ values (0.39 and 2.2 mmol COOH/g cellulose) we report in this contribution for the post-oxidized TOCN (sample TOCN-P) are the highest values reported so far for TEMPO carboxylated nanocellulose following Saito and Isogai´s post oxidation procedure (Isogai et al. 2010; Mishra et al. 2012; Isogai 2013; Rohaizu and Wanrosli 2017; Lin et al. 2018; Zhou et al. 2018; Huang et al. 2019; Isogai and Zhou 2019). We also calculated the approximate amount of oxidized anhydroglucose units (AGU) from the σ values (mol COOH/mol cellulose) and found that out of 1000 AGU 356 were oxidized to the corresponding uronic acid by combining TEMPO oxidation and $NaClO_2$ post-oxidation (TOCN-P). In contrast, TEMPO nanocellulose (TOCN) has 254 oxidized units (Saito et al. 2006). After the amidation reaction we observe a 73% and 82% decrease in carboxylate content for TOCN-ODA and TOCN-P-ODA with respect to TOCN and TOCN-P. These values can be related with the degree of coupling (DC) leading to amide formation, i.e., about 1.14 and 1.80 mmol of amide units were coupled per gram of cellulose, respectively. A similar DC value (up to 70%) was reported by our group, using microcrystalline cellulose as TOCN source (Gómez et al. 2017).

Z (ζ) potential is an indicator of colloidal dispersion stability. For aqueous suspensions of TOCN, stability depends on the electrostatic repulsion between the surface's anionic groups. When the suspension has a high potential value (ζ between − 40 and − 80 mV), it is electrically stabilized over time and resists aggregation. Conversely, if the attractive forces exceed the repulsive forces (ζ from 0 to − 30 mV) the dispersion tends to flocculate and precipitate (Wicaksono et al. 2013). ζ-potential values for TOCN and TOCN-P were − 56 mV and − 64 mV, indicating stable aqueous dispersions of the materials. The values also support the conductometric results which relate to an increase in the amount of carboxylate groups after post-oxidation of TOCN. On the other hand, ζ-potential values decreased 34% and 52% after the amidation reaction, to − 37 mV and − 31 mV, indicating low stability over time for TOCN-ODA and TOCN-P-ODA.

We tested the hydrophobic character of TOCN-ODA and TOCN-P-ODA by means of dispersion tests in non-polar organic solvents such as toluene. Figure 4a shows that when water was used as solvent, TOCN and TOCN-P formed translucent suspensions stable up to 3 months. However, the same materials readily precipitate in toluene (Fig. 4b). Aqueous dispersions of these polar materials are very stable due to electrostatic Coulombic repulsion between abundant negative charges on the CNF's surface; osmotic effects or a combination of both effects (Okita et al. 2011). After amidation, a certain amount of TOCN-ODA and TOCN-P-ODA could be dispersed in water, however, most of the material migrated to the surface as seen in Fig. 4c. Conversely, the hydrophobic materials formed stable, homogeneous and opaque dispersions in toluene (Fig. 4d).

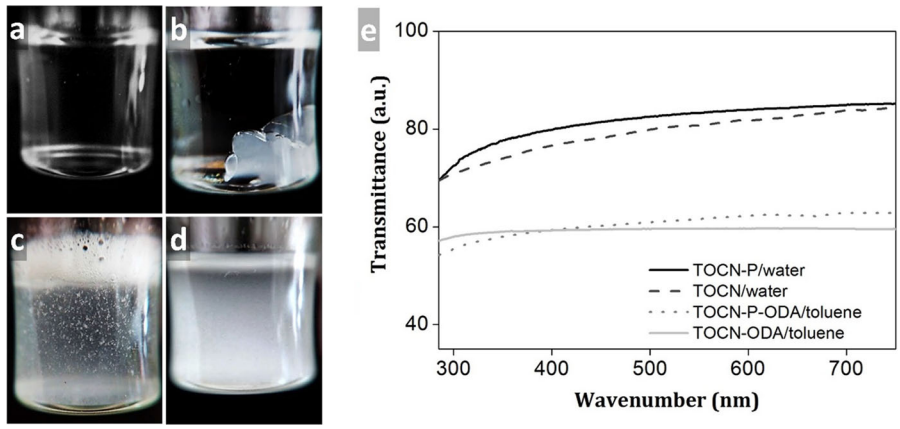

Fig. 4 Images of **a** TOCN/water, **b** TOCN/toluene, **c** TOCN-ODA/water, **d** TOCN-ODA/toluene and **e** transmittance spectra of TOCN-(P) in water and TOCN-(P)-ODA in toluene dispersions

Figure 4e shows the transmittance spectra in the visible region, of the materials forming stable dispersions in water and toluene. TOCN and TOCN-P form stable dispersions in water with transmittances up to 80%; TOCN-ODA and TOCN-P-ODA form stable dispersions in toluene with transmittances up to 60%. For aqueous solutions of carboxylated nanocellulose (TOCN and TOCN-P) light transmission depends on the content of carboxylate, i.e. the higher the σ the more translucent the solution. In other words, a higher content of anionic groups on the surface of TOCN will result in increased repulsion between the dispersed particles, inhibiting aggregation and making the solution more transparent (Besbes et al. 2011). Chen and co-workers observed the same trend in the transmittance of TOCN suspensions prepared from bleached pulps (Chen et al. 2017). On the other hand, for the toluene dispersions of the amidated products (TOCN-ODA and TOCN-P-ODA) there is a significant reduction in transmittance, when compared with their aqueous counterparts. This phenomenon may be caused by lowering of the surface's charge, as a result of hydrophobization, that in turn increases the probability of interaction and aggregation between the nanofibers. Light scattering, with a significant reduction in transmittance, occurs upon interaction of these aggregates with a light source (Besbes et al. 2011; Fukuzumi 2012).

Surface-active properties

TOCN-ODA and TOCN-P-ODA are structurally similar to a surfactant, with hydrophilic heads in the form of COOH and OH groups in the anhydroglucose units, and hydrophobic tails corresponding to aliphatic octadecyl chains. The interfacial behavior of these materials can be determined by calculating their hydrophilic-lipophilic balance (HLB). The HLB scale varies from zero to twenty, where a value of zero corresponds to a totally hydrophobic structure and twenty indicates a completely hydrophilic molecule. HLB can be determined experimentally or theoretically. A theoretical calculation can be performed using Griffin's mathematical method (Griffin 1949), as follows:

$$HLB = 20 * (M_h/M_m) \tag{5}$$

where M_h is the molecular weight of the hydrophilic groups and M is the molecular weight of the whole molecule. To calculate the HLB value of the TOCN before and after surface modification, Eq. (5) transforms into:

$$HLB = 20 * \left[\left(\sum M_{hi} * n_i\right) + \left(\sum M_{hj} * n_j\right) + \left(\sum M_{hk} * n_k\right) + \left(\sum M_{hl} * n_l\right)\right] \Big/ \left[(M_{mi} * n_i) + (M_{mj} * n_j) + (M_{mk} * n_k) + (M_{ml} * n_l)\right] \tag{6}$$

where M_{hi}, M_{hj}, M_{hk} and M_{hl} represent the sum of the molecular weights of the hydrophilic groups (–OH, –O–, –COH, –COOH and –CONH) in the anhydroglucose units depending upon oxidation and/or grafting, *e.g.* (*i*) corresponds to C6–OH moieties, (*j*) represents incomplete oxidation or –COH units, (*k*) indicates complete oxidation or –COOH groups, (*l*) corresponds to $–CONH(CH_2)_{17}CH_3$ groups in the amidated

samples and n is equivalent to the number of AGU units within each kind of group. n can be calculated from the C6-oxidized AGU/1000 AGU distribution reported in Table 1; for instance, for TOCN out of 1000 AGU units, 644 units were not oxidized after the reaction with TEMPO (equivalent to n_i), 102 units were incompletely oxidized (equivalent to n_j, calculated as the difference between 356 oxidized units of the TOCN-P after post-oxidation and the 254 completely oxidized units of the TOCN from TEMPO) and 254 units were completely oxidized (corresponding to n_k). n_l is equal to zero due to the absence of amide bonds. M_m is the sum of the products of the molecular weights of the AGU units according to their oxidation and/or grafting and n_i, n_j, n_k and n_l.

Using Eq. 6, HLB values of 11.04 and 11.13 were obtained for TOCN and TOCN-P, respectively, (see Table 2). These values correspond to those of hydrophilic o/w surfactants, or emulsifying agents with high affinity for polar phases. In fact, while Fig. 4a shows a stable water dispersion of TOCN Fig. 4b demonstrates that the same material does not interact with an organic non-polar solvent such as toluene. The amidated products, TOCN-ODA and TOCN-P-ODA, have theoretical HLB values of 8.59 and 7.68. These values indicate that TOCN-ODA and TOCN-P-ODA can act as wetting/spreading agents with poor dispersibility (unstable) in water (Gadhave 2014; Zheng, Yan et al. 2015). Figures 4c and 4d illustrate this behavior showing that the TOCN-ODA specimen does not disperse in water while it does in toluene.

Contact angle (CA) refers to the angle formed between a solid surface and a liquid, typically water. The CA value depends on the cohesive forces of the water droplet and the adhesive forces between the outline of the contact surface and the liquid (Benkaddour et al. 2014). CA values between 0° and 90° indicate hydrophilic surfaces where the prevailing forces are adhesive. We observed a low CA of 24° and 21° for TOCN and TOCN-P films in contact with water (Fig. 1 and Table 2). The high hydrophilic nature of TOCN and TOCN-P is due to the abundance polar groups (–OH and –COOH) in their surface (Benkaddour et al. 2014). On the other hand, CA values between 90° and 180° indicate hydrophobic surfaces where the prevailing forces are cohesive. We observed CA of 126° and 130° for TOCN-ODA and TOCN-P-ODA films in contact with water (Fig. 1 and Table 2). The dramatic change in CA of the amidated products, when compared with TOCN and TOCN-P, can be attributed to the presence of nonpolar octadecylamine alkyl chains coupled to the surface of the nanocellulose after the amidation reaction and the surface roughness of the nanocellulose films. Hydrophobicity can be achieved by surface roughness (micro and nano hierarchical structures), low surface energy materials, or combinations thereof (He et al. 2013). Benkaddour and coworkers reported similar results for the hydrophobization of TEMPO-oxidized cellulose gels when amidated with stearyl amine (SA) using carbodiimide and hydroxysuccimide as catalysts. The authors reported that initially, the TOCN gel exhibited a high hydrophilic character (CA 41°), which increased to a CA of 102° in compressed nanofiber films (smooth surface) after hydrophobization and to around 150° for lyophilized films (rough surface). These results demonstrate the influence of surface roughness in achieving a transition from a

Table 2 HLB, CA and SFE (dispersive, polar, and total) of Fique tow TOCN, TOCN-P, TOCN-ODA and TOCN-P-ODA

Material	HLB	CA (°)			γ_s^d	γ_s^p	γ_s
		H_2O	CH_2I_2	$C_3H_8O_3$	(mJ/m^2)	(mJ/m^2)	(mJ/m^2)
TOCN	11.04	24	35	12	26.66	39.66	66.32
TOCN-P	11.13	21	32	10	27.38	40.09	67.46
TOCN-ODA	8.59	126	97	115	10.17	3.97×10^{-5}	10.17
TOCN-P-ODA	7.68	130	104	119	7.71	3.17×10^{-4}	7.71

γ^d dispersive component of SFE

γ^p polar component of SFE

γ total SFE

hydrophobic to a superhydrophobic surface (Benkaddour et al. 2014). Although in our work the CA values for TOCN-ODA and TOCN-P-ODA films are very high, they cannot be classified as superhydrophobic (CA > 150°) materials. Most organic superhydrophobic materials are currently based on fluorine- or silicon- containing moieties. Herein we demonstrate that amidation of oxidized and post-oxidized nanocellulose fibers effectively decreases the surface free energy (SFE) of the material, which may be a good starting point for developing new fluorine/silicon – free superhydrophobic materials.

Surface free energy (SFE) is an essential criterion for studying interfacial properties of materials (e.g., wettability, adhesion). SFE can be measured according to the Young equation ($\gamma_S = \gamma_{SL} + \gamma_L \cos \Theta$) where γ_S is the SFE of the solid, γ_{SL} is the SFE at the liquid–solid interface, γ_L is the SFE of the liquid and Θ the contact angle between solid and liquid. This equation was derived from the condition of equilibrium of forces that represent surface tensions at the contact point of three phases—solid, liquid and gas (Rudawska 2009). Several approaches exist to solve the Young equation. We used the Owens, Wendt, Rabel and Kaelble approach (also known as OWRK-model) to calculate total SFE for the materials reported in this contribution. The OWRK method allows calculation of the polar and dispersive components of a solid SFE using experimental CA values of several liquids with the material of study. The OWRK method is particularly useful when studying the role of dispersive and polar components of the SFE in wettability and adhesion; hence, its use is adequate in our case because we are testing the effect of surface polarity changes in nanocelluloses.

The OWRK equation can be expressed in the linear form:

$$\frac{\gamma_l(1+\cos\theta)}{2\sqrt{\gamma_l^d}} = \sqrt{\gamma_s^p} * \sqrt{\frac{\gamma_l^p}{\gamma_l^d}} + \sqrt{\gamma_s^d} \quad (7)$$

where the total SFE is equal to the sum of the polar and dispersive SFE components of a solid (s) or a liquid (l), i.e. $\gamma_s = \gamma_s^p + \gamma_s^d$ and $\gamma_l = \gamma_l^p + \gamma_l^d$.

From the axis intercept and the slope of the curve $\gamma_l(1+\cos\theta)/2\sqrt{\gamma_l^d}$ *vs* $\sqrt{\gamma_l^p}/\sqrt{\gamma_l^d}$, the dispersive and polar parts of the solid's surface energy can be calculated, respectively.

Using our experimental CA data for TOCN, TOCN-P, TOCN-ODA, and TOCN-P-ODA at the at the sample/water/diiodomethane/glycerol interfaces (Table 2) and γ_l^p and γ_l^d values for water, diiodomethane and glycerol (Table S2), we calculated the materials SFE using the OWRK approach (Table 2). High SFE values are characteristic of hydrophilic surfaces, and we obtained values of 66.32 and 67.46 mJ/m^2 for TOCN, TOCN-P. These values lie within the ranges reported by several authors for nanocelluloses (SFE values between 50 and 70 mJ/m^2 for hydrophilic nanocrystals and nanofibers) (Khoshkava and Kamal 2013; Sun et al. 2018). In TOCN and TOCN-P the polar component (representing Coulombic interactions between permanent and induced dipoles, *i.e.* hydrogen bonding, inductive, and acid–base interactions) exceeds the dispersive component of the SFE indicating highly hydrophilic materials. Upon surface amidation, SFE values drop to 10.17 and 7.71 mJ/m^2 for TOCN-ODA and TOCN-P-ODA, respectively. These nanocelluloses exhibit high dispersive components (representing van der Waals interactions) exceeding the polar component of the SFE, indicating low polarity (hydrophobic) materials. Several authors report low total SFE values for hydrophobic nanocelluloses, between 10 and 13 mJ/m^2 for water CA ~ 130°, using the Owens and Wendt method (Bashar et al. 2017; Hasan et al. 2019).

Thermal behavior of nanocelluloses

Thermogravimetric analysis (TGA) was used to evaluate the thermal degradation process of cellulose samples, and the results are shown in Fig. 5. The possible thermal degradation paths of cellulose involve dehydration to form anhydrocellulose, and depolymerization to yield levoglucosan, which forms tar above 400 °C (Lichtenstein and Lavoine 2017). Thermogravimetric curves (TG) and their corresponding derivative (DTG) curves show weight losses for all TOCN samples in the 40 °C to 200 °C temperature range, due to loosely bound water evaporation. Interestingly, TOCN-ODA and TOCN-P-ODA exhibit less adsorbed water than TOCN and TOCN-P. Apparently, increasing hydrophobic interactions at the nanofibril surface dramatically reduces moisture sensitivity as in TOCN-ODA and TOCN-P-ODA (Cunha et al. 2007). On the other hand, TOCN-P adsorbs the most water which is explained by the

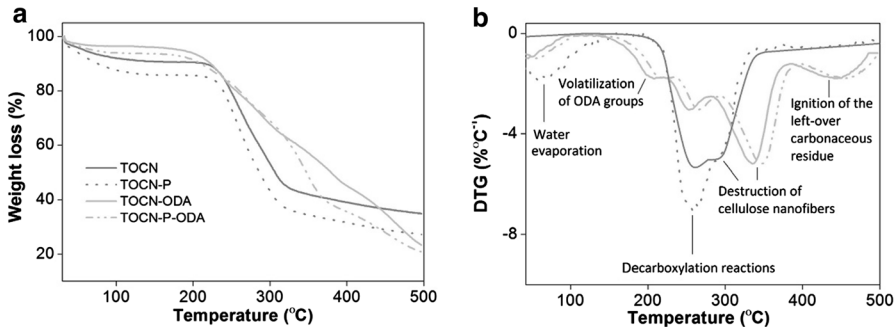

Fig. 5 Thermogravimetric behavior of Fique tow: TOCN, TOCN-P, TOCN-ODA and TOCN-P-ODA. **a** TG and **b** DTG curves

high degree of oxidation and high surface charge of this material (Table 1). Regarding the second event (peaks at 185 and 195 °C for TOCN-ODA and TOCN-P-ODA,), we hypothesize a decomposition event related to volatilization of ODA groups.

After water loss, thermal degradation of unmodified TOCN and TOCN-P follows with decarboxylation reactions and deep dehydration of the cellulose chains between 220 °C and 280 °C with a corresponding weight loss of 19.66% and 24.91%. This process is followed by formation of carbonyl compounds and the beginning of an aromatization process (Lichtenstein and Lavoine 2017). The next step is the collapse of the glycosidic structure between 280 °C and 350 °C with a weight loss of 27.06% and 24.01%, involving the destruction of crystalline and amorphous regions of the cellulose nanofibers with the formation of D-glucopyranose monomers that will further decompose into carboxylic compounds (Fukuzumi et al. 2010). The presence of the carboxylate groups in TOCN and TOCN-P materials causes the degradation temperature of the cellulose to drop (296 °C and 293 °C, respectively) in comparison with that of the starting material (340 °C for delignified Fique tow, Figure S4 Supporting Information) (Ovalle-Serrano et al. 2018a).

TGA results indicate a higher thermal stability for the hydrophobic derivatives TOCN-ODA and TOCN-P-ODA than for the hydrophilic TOCN and TOCN-P (Cunha et al. 2007). From an initial decomposition temperature of 296 °C and 293 °C for TOCN and TOCN-P, TOCN-ODA and TOCN-P-ODA decompose at 335 °C and 348 °C, respectively. This effect can be explained by the ability of the long chains of ODA to organize themselves on the surface of the TEMPO-oxidized fibers forming a protecting "shell" (Missoum et al. 2012). Higher thermal stability was observed for TOCN-P-ODA than for TOCN-ODA which can be explained by the greater degree of coupling after the amidation process. Missoum and wo-workers also observed a similar effect when they grafted octadecyl isocyanate on NFC. In their report, the hydrophobic samples exhibited improved thermal resistance, from 241 °C for raw NFC up to 331 °C after surface modification with octadecyl isocyanate. The authors suggested that octadecyl isocyanate chains protect NFC by hindering accessibility to the cellulosic core (Missoum et al. 2012). In our case, we believe the octadecyl units grafted onto the TOCN have a similar shielding effect. This effect is evident as an increase in thermal stability, equivalent to 39 °C, from TOCN to TOCN-ODA, and to 55 °C from TOCN-P to TOCN-P-ODA.

Conclusions

We investigated the effect of post-oxidation reactions in TOCN (obtained from Fique tow) on the hydrophobization of these materials via amidation reactions. TOCN exhibit a network-like morphology and high values of carboxylate content, 0.29, that increased up to 0.39 after post-oxidation (TOCN-P). High ζ-potential values, -56 and -64 eV for TOCN and TOCN-P, indicate high stability of these materials in aqueous suspensions. Theoretical HLB values of 11.04 and 10.45 for TOCN and TOCN-P indicate a potential use for these materials as hydrophilic o/w surfactants or emulsifying agents with high affinity for polar phases. CA of 24° and 21° for TOCN and TOCN-P films highlight the high hydrophilic nature

of these materials, due to abundant polar groups (-OH and –COOH) in their surface. After amidation, we observed that the more hydrophilic the starting material the more hydrophobic the amidated product will be. This effect is observed in an increased degree of coupling after amidation: from 0.22 for TOCN-ODA up to 0.33 for TOCN-P-ODA. In addition, TOCN-ODA and TOCN-P-ODA are able to form stable dispersions in toluene and exhibit theoretical HLB values of 8.59 and 7.68, indicating their ability to act as wetting/spreading agents with poor dispersibility in water. CA of 126° and 130° for TOCN-ODA and TOCN-P-ODA films illustrate the effect of the octadecylamine alkyl chains on the hydrophobic properties of the nanocellulose surface. Finally, thermograms indicate that amidation reactions can effectively shield the nanocellulose surface from thermal degradation from initial decomposition temperatures of 296 °C and 288 °C for "naked" TOCN and TOCN-P to 335 °C and 348 °C for the "protected" amidated products (TOCN-ODA and TOCN-P-ODA, respectively).

Acknowledgments We thank Guatiguará Technology Park and the Central Research Laboratory Facility (X-ray and microscopy laboratories) at Universidad Industrial de Santander for infrastructural support. We thank Professor Juan Hinestroza director of the Textiles Nanotechnology Lab, College of Human Ecology, Cornell University for TEM analyses and discussion; we also acknowledge use of the Cornell Center for Materials Research Shared Facilities which are supported through the NSF MRSEC program (DMR-1719875) and an INVEST grant via the Cornell Center for Materials Research (M01-1985) for TEM analyses. We thank Andrés J. Calderón, Ph.D. for assistance with numerical computations for SFE calculations. We also acknowledge a graduate fellowship from COLCIENCIAS Program No. 567/2012 and financial support from Universidad Industrial de Santander Vice-chancellor for Research Office (Grant 2316/2017).

References

Akira Isogai TS, Saito T, Fukuzumi H (2011) TEMPO-oxidized cellulose nanofibers. Nanoscale 3:71–85

Bashar MM, Zhu H, Yamamoto S, Mitsuishi M (2017) Superhydrophobic surfaces with fluorinated cellulose nanofiber assemblies for oil-water separation. RSC Adv 7:37168–37174. https://doi.org/10.1039/c7ra06316d

Benkaddour A, Journoux-Lapp C, Jradi K et al (2014) Study of the hydrophobization of TEMPO-oxidized cellulose gel through two routes: amidation and esterification process. J Mater Sci 49:2832–2843. https://doi.org/10.1007/s10853-013-7989-y

Besbes I, Alila S, Boufi S (2011) Nanofibrillated cellulose from TEMPO-oxidized eucalyptus fibres: effect of the carboxyl content. Carbohydr Polym 84:975–983. https://doi.org/10.1016/j.carbpol.2010.12.052

Besemer A (1993) The bromide catalized hypochlorite oxidation of starch and inulin. Delft University of Technology

Bhatnagar A (2005) Processing of Cellulose Nanofiber-reinforced Composites. J Reinf Plast Compos 24:1259–1268. https://doi.org/10.1177/0731684405049864

Bledzki AK, Mamun AA, Lucka-Gabor M, Gutowski VS (2008) The effects of acetylation on properties of flax fibre and its polypropylene composites. Express Polym Lett 2:413–422. https://doi.org/10.3144/expresspolymlett.2008.50

Bragd PL, Besemer AC, Van Bekkum H (2000) Bromide-free TEMPO-mediated oxidation of primary alcohol groups in starch and methyl α-D-glucopyranoside. Carbohydr Res 328:355–363. https://doi.org/10.1016/S0008-6215(00)00109-9

Chen W, Yu H, Liu Y et al (2011) Individualization of cellulose nanofibers from wood using high-intensity ultrasonication combined with chemical pretreatments. Carbohydr Polym 83:1804–1811. https://doi.org/10.1016/j.carbpol.2010.10.040

Chen Y, Geng B, Ru J et al (2017) Comparative characteristics of TEMPO-oxidized cellulose nanofibers and resulting nanopapers from bamboo, softwood, and hardwood pulps. Cellulose 24:4831–4844. https://doi.org/10.1007/s10570-017-1478-4

Cunha AG, Freire CSR, Silvestre AJD et al (2007) Highly hydrophobic biopolymers prepared by the surface pentafluorobenzoylation of cellulose substrates. Biomacromol 8:1347–1352. https://doi.org/10.1021/bm0700136

Dai L, Wang B, Long Z et al (2015) Properties of hydroxypropyl guar/TEMPO-oxidized cellulose nanofibrils composite films. Cellulose 22:3117–3126. https://doi.org/10.1007/s10570-015-0691-2

David R, Williams KN (1980) A mild oxidation of aldehydes to α, β-unsaturated aldehydes. Tetrahedron Lett 21:4417–4420

Davidson TC, Newman RH, Ryan MJ (2004) Variations in the fibre repeat between samples of cellulose I from different sources. Carbohydr Res 339:2889–2893. https://doi.org/10.1016/j.carres.2004.10.005

French AD (2014) Idealized powder diffraction patterns for cellulose polymorphs. Cellulose 21:885–896. https://doi.org/10.1007/s10570-013-0030-4

Fukuzumi H (2012) Studies on structures and properties of TEMPO-oxidized cellulose nanofibril films. 博士論文 98

Fukuzumi H, Saito T, Okita Y, Isogai A (2010) Thermal stabilization of TEMPO-oxidized cellulose. Polym Degrad Stab 95:1502–1508. https://doi.org/10.1016/j.polymdegradstab.2010.06.015

Gadhave A (2014) Determination of Hydrophilic-Lipophilic Balance Value. 3:573–575

Gert EV, Torgashov VI, Zubets OV, Kaputskii FN (2005) Preparation and properties of enterosorbents based on

carboxylated microcrystalline cellulose. Cellulose 12:517–526. https://doi.org/10.1007/s10570-005-7134-4
Gómez FN, Combariza MY, Blanco-Tirado C (2017) Facile cellulose nanofibrils amidation using a 'one-pot' approach. Cellulose 24:717–730. https://doi.org/10.1007/s10570-016-1174-9
Griffin WC (1949) Classification of surface active agents by HLB. J Soc Cosmet Chem 1:311–315
Habibi Y, Chanzy H, Vignon MR (2006) TEMPO-mediated surface oxidation of cellulose whiskers. Cellulose 13:679–687. https://doi.org/10.1007/s10570-006-9075-y
Hasan M, Gopakumar DA, Arumughan V et al (2019) Robust superhydrophobic cellulose nanofiber aerogel for multifunctional environmental applications. Polymers (Basel) 11:1–14. https://doi.org/10.3390/polym11030495
He M, Xu M, Zhang L (2013) Controllable Stearic Acid Crystal Induced High Hydrophobicity on Cellulose Film Surface. https://doi.org/10.1021/am3026536
He M, Lu A, Zhang L (2014) Advances in cellulose hydrophobicity improvement. In: Food additives and packaging. ACS Symposium, pp 241–274
Huang CF, Tu CW, Lee RH et al (2019) Study of various diameter and functionality of TEMPO-oxidized cellulose nanofibers on paraquat adsorptions. Polym Degrad Stab 161:206–212. https://doi.org/10.1016/j.polymdegradstab.2019.01.023
Iskalieva A, Yimmou BM, Gogate PR et al (2012) Cavitation assisted delignification of wheat straw: a review. Ultrason Sonochem 19:984–993. https://doi.org/10.1016/j.ultsonch.2012.02.007
Isogai A (2013) Wood nanocelluloses: fundamentals and applications as new bio-based nanomaterials. J Wood Sci 59:449–459. https://doi.org/10.1007/s10086-013-1365-z
Isogai A, Zhou Y (2019) Diverse nanocelluloses prepared from TEMPO-oxidized wood cellulose fibers: nanonetworks, nanofibers, and nanocrystals. Curr Opin Solid State Mater Sci 23:101–106. https://doi.org/10.1016/j.cossms.2019.01.001
Isogai T, Saito T, Isogai A (2010) TEMPO electromediated oxidation of some polysaccharides including regenerated cellulose fiber. Biomacromol 11:1593–1599. https://doi.org/10.1021/bm1002575
Isogai A, Hänninen T, Fujisawa S, Saito T (2018) Progress in Polymer Science Review: catalytic oxidation of cellulose with nitroxyl radicals under aqueous conditions. Prog Polym Sci 86:122–148. https://doi.org/10.1016/j.progpolymsci.2018.07.007
Johnson RK, Zink-Sharp A, Glasser WG (2011) Preparation and characterization of hydrophobic derivatives of TEMPO-oxidized nanocelluloses. Cellulose 18:1599–1609. https://doi.org/10.1007/s10570-011-9579-y
Kato Y, Matsuo R, Isogai A (2003) Oxidation process of water-soluble starch in TEMPO-mediated system. 51:69–75
Khoshkava V, Kamal MR (2013) Effect of surface energy on dispersion and mechanical properties of polymer/nanocrystalline cellulose nanocomposites. Biomacromol 14:3155–3163. https://doi.org/10.1021/bm400784j
Lasseuguette E (2008) Grafting onto microfibrils of native cellulose. Cellulose 15:571–580. https://doi.org/10.1007/s10570-008-9200-1
Lichtenstein K, Lavoine N (2017) Toward a deeper understanding of the thermal degradation mechanism of nanocellulose. Polym Degrad Stab 146:53–60. https://doi.org/10.1016/j.polymdegradstab.2017.09.018
Lif A, Stenstad P, Syverud K et al (2010) Fischer-Tropsch diesel emulsions stabilised by microfibrillated cellulose and nonionic surfactants. J Colloid Interface Sci 352:585–592. https://doi.org/10.1016/j.jcis.2010.08.052
Lin C, Zeng T, Wang Q et al (2018) Effects of the conditions of the TEMPO/NaBr/NaClO system on carboxyl groups, degree of polymerization, and yield of the oxidized cellulose. BioResources 13:5965–5975
Mandal A, Chakrabarty D (2011) Isolation of nanocellulose from waste sugarcane bagasse (SCB) and its characterization. Carbohydr Polym 86:1291–1299
Mishra SP, Manent AS, Chabot B, Daneault C (2012) The use of sodium chlorite in post-oxidation of TEMPO-oxidized pulp: effect on pulp characteristics and nanocellulose yield. J Wood Chem Technol 32:137–148. https://doi.org/10.1080/02773813.2011.624666
Missoum K, Bras J, Belgacem MN (2012) Organization of aliphatic chains grafted on nanofibrillated cellulose and influence on final properties. Cellulose 19:1957–1973. https://doi.org/10.1007/s10570-012-9780-7
Morán JI, Alvarez VA, Cyras VP, Vázquez A (2008) Extraction of cellulose and preparation of nanocellulose from sisal fibers. Cellulose 15:149–159. https://doi.org/10.1007/s10570-007-9145-9
Okita Y, Saito T, Isogai A (2010) Entire surface oxidation of various cellulose microfibrils by TEMPO mediated oxidation. Biomacromolecules 11:1696–1700
Okita Y, Fujisawa S, Saito T, Isogai A (2011) TEMPO-oxidized cellulose nanofibrils dispersed in organic solvents. Biomacromol 12:518–522. https://doi.org/10.1021/bm101255x
Ovalle-Serrano SA, Blanco-Tirado C, Combariza MY (2018a) Exploring the composition of raw and delignified Colombian fique fibers, tow and pulp. Cellulose 25:151–165. https://doi.org/10.1007/s10570-017-1599-9
Ovalle-Serrano SA, Gómez FN, Blanco-Tirado C, Combariza MY (2018b) Isolation and characterization of cellulose nanofibrils from Colombian Fique decortication by-products. Carbohydr Polym 189:169–177. https://doi.org/10.1016/j.carbpol.2018.02.031
Rodionova G, Eriksen Gregersen (2012) TEMPO-oxidized cellulose nanofiber films: effect of surface morphology on water resistance. Cellulose 19:1115–1123. https://doi.org/10.1007/s10570-012-9721-5
Rohaizu R, Wanrosli WD (2017) Sono-assisted TEMPO oxidation of oil palm lignocellulosic biomass for isolation of nanocrystalline cellulose. Ultrason Sonochem 34:631–639. https://doi.org/10.1016/j.ultsonch.2016.06.040
Rudawska A, Jacniacka E (2009) Analysis for determining surface free energy uncertainty by the Owen – Wendt method. Int J Adhes Adhes 29:451–457. https://doi.org/10.1016/j.ijadhadh.2008.09.008
Saito T, Isogai A (2004) TEMPO-mediated oxidation of native cellulose. The effect of oxidation conditions on chemical and crystal structures of the water-insoluble fractions. Biomacromol 5:1983–1989. https://doi.org/10.1021/bm0497769

Saito T, Yanagisawa M, Isogai A (2005) TEMPO-mediated oxidation of native cellulose: SEC–MALLS analysis of water-soluble and -insoluble fractions in the oxidized products. Cellulose 12:305–315. https://doi.org/10.1007/s10570-004-5835-8

Saito T, Okita Y, Nge TT et al (2006) TEMPO-mediated oxidation of native cellulose: microscopic analysis of fibrous fractions in the oxidized products. Carbohydr Polym 65:435–440. https://doi.org/10.1016/j.carbpol.2006.01.034

Saito T, Kimura S, Nishiyama Y, Isogai A (2007) Cellulose nanofibers prepared by TEMPO-mediated oxidation of native cellulose. Biomacromol 8:2485–2491. https://doi.org/10.1021/bm0703970

Sèbe G, Ham-Pichavant F, Ibarboure E et al (2012) Supramolecular structure characterization of cellulose II nanowhiskers produced by acid hydrolysis of cellulose I substrates. Biomacromol 13:570–578. https://doi.org/10.1021/bm201777j

Segal L, Creely JJ, Martin AE, Conrad CM (1959) An empirical method for estimating the degree of crystallinity of native cellulose using the x-ray diffractometer. Text Res J 29:786–794. https://doi.org/10.1177/004051755902901003

Sehgal DVI (1994) A method for the high efficiency of water-soluble carbodiimide-mediated amidation. Anal Biochem 218:87–91

Smith KC, Edionwe E, Michel B (2010) Conductimetric titrations: a predict-observe-explain activity for general chemistry. J Chem Educ 87:1217–1221. https://doi.org/10.1021/ed100538q

Sun B, Gu CJ, Ma JH, Liang BR (2005) Kinetic study on TEMPO-mediated selective oxidation of regenerated cellulose. Cellulose 12:59–66

Sun X, Mei C, French AD et al (2018) Surface wetting behavior of nanocellulose-based composite films. Cellulose 25:5071–5087. https://doi.org/10.1007/s10570-018-1927-8

Tang Z, Li W, Lin X et al (2017) TEMPO-Oxidized cellulose with high degree of oxidation. Polymers (Basel) 9:3–4. https://doi.org/10.3390/polym9090421

Wada M, Kondo T, Okano T (2003) Thermally induced crystal transformation from cellulose I[alpha] to I[beta]. Polym J 35:155–159. https://doi.org/10.1295/polymj.35.155

Wicaksono R, Syamsu K, Yuliasih I, Nasir M (2013) Cellulose nanofibers from cassava bagasse: characterization and application on tapioca-film. Chem Mater Res 3:79–87

Xiao S, Gao R, Lu Y et al (2015) Fabrication and characterization of nanofibrillated cellulose and its aerogels from natural pine needles. Carbohydr Polym 119:202–209

Xu Y, Kawata S, Hosoi K et al (2009) Thermomechanical properties of the silanized-kenaf/polystyrene composites. Express Polym Lett 3:657–664. https://doi.org/10.3144/expresspolymlett.2009.82

Yang H (2011) Investigation and characterization of oxidized cellulose and cellulose nanofiber films. Master thesis, McGill University, Canada

Zenkiewicz M (2006) New method of analysis of the surface free energy of polymeric materials calculated with Owens-Wendt and Neumann methods. Polimery/Polymers 51:584–587

Zheng Y, Zheng M, Ma Z et al (2015) Sugar fatty acid esters. In: Polar lipids: biology, chemistry, and technology. AOCS Press, pp 215–243

Zhou Y, Saito T, Bergström L, Isogai A (2018) Acid-free preparation of cellulose nanocrystals by TEMPO oxidation and subsequent cavitation. Biomacromol 19:633–639. https://doi.org/10.1021/acs.biomac.7b01730